

## DISTANCES TO EXTRAGALACTIC SUPERNOVAE

ROBERT P. KIRSHNER

Hale Observatories, California Institute of Technology, Carnegie Institution of Washington

AND

JOHN KWAN

Institute for Advanced Study

Received 1974 April 1; revised 1974 May 6

### ABSTRACT

Distances to the Type II supernovae 1969I in NGC 1058 and SN 1970g in M101 are determined through Baade's method for variable stars. The photospheric temperatures are derived from spectrophotometric scans and from broad-band photometry. A model of line formation is used to relate the velocity of the material at the photosphere to observed line shapes in spectra and scans. These results are used to estimate a distance of  $12 \pm 3$  Mpc to NGC 1058 and  $6 \pm 3$  Mpc to M101. If the redshifts of these two nearby galaxies are proportional to distance, then  $H_0 = 60 \pm 15$  km s<sup>-1</sup> Mpc<sup>-1</sup>.

*Subject headings:* cosmology — galaxies — supernovae

### I. INTRODUCTION

The extragalactic distance scale depends on distances established within the Local Group, and within our own Galaxy through variable stars and main-sequence fitting. Ultimately, the stellar distance scale is tied to locally determined parallaxes, and in particular to the distance to the Hyades (Sandage 1956).

This paper outlines a method for determining extragalactic distances from observations of supernovae. It is independent of all distances determined in our Galaxy, or in the Local Group, and it does not even assume that the observed events are of the same absolute magnitude.

On inspection of recent photometric scans of supernovae (Kirshner *et al.* 1973, hereafter referred to as KOPS), L. Searle suggested that the expansion of the photosphere, as determined from the temperature and apparent magnitude, could be linked to the expansion velocities observed in lines to estimate the distance to a supernova through Baade's (1926) method for variable stars.

When the energy distribution of the continuum is accurately characterized by a temperature  $T$ , the received flux density,  $f_v$ , determines the angular size of the emitter,  $\theta = R/D$ , viz.

$$\theta = [f_v/\pi B_v(T)]^{1/2}. \quad (1)$$

Here  $R$  is the radius of the photosphere,  $D$  is the distance to the supernova, and  $B_v(T)$  is the Planck function. Thus the distance is determined by measurements of  $f_v$ ,  $T$ , and  $R$ . Both  $f_v$  and  $T$  can be estimated directly.  $R$  is estimated by the following method.

In the simplest kinematic assumption the envelope undergoes free expansion once the shock emerges from the surface of the star. Gravitational deceleration and radiation pressure both produce velocity changes much smaller than the initial velocities imparted by the shock (Sakurai 1960; Grassberg, Imshennik, and Nadyozhin

1971). The pressure due to the interstellar medium is negligible because the amount of matter swept up by the supernova in a few months is very small, perhaps  $10^{25}$  g. If at some instant,  $t$ , the velocity of the material at the photosphere,  $v$ , is determined, and the time,  $t_0$ , at which the envelope started expanding is known, then given free expansion, the radius of the photosphere is

$$R = v(t - t_0) + R_0. \quad (2)$$

The initial radius of the envelope is denoted by  $R_0$ , and it is assumed that when the envelope begins to expand, most of the material is located near  $R_0$ .

Usually, the photospheric radius becomes greater than the initial radius  $R_0$  after a relatively short time (cf. § II) and  $R_0$  can be ignored in the distance determination. The time of initial expansion  $t_0$ , however, is crucial to the distance determination. If a good estimate of  $t_0$  cannot be obtained, then two sets of values of  $v$ ,  $T$ , and  $f_v$  must be used, separated by a sufficient span of time.

It is easily shown, in this case, that the distance is

$$D = \frac{v_2(t_2 - t_1) + R_0(1 - v_2/v_1)}{\theta_2 - (\theta_1 v_2/v_1)}. \quad (3)$$

The difficulties of this method occur in estimating the temperature in equation (1), and the velocity in equation (2). In § II of this paper the temperatures for the supernovae 1969I and 1970g are derived directly from spectrophotometric scans when they are available, and otherwise indirectly from broad-band photometry. The velocities are inferred from the observed line profiles in § III. The distances to NGC 1058 and M101 are derived in § IV. Finally, in § V the accuracy of the results is discussed and a summary is presented of appropriate procedures to be undertaken in future applications of this method.

TABLE 1  
SUPERNOVA OBSERVATIONS

Date (UT)	Julian Date – 2,440,000	Plate	Observer	Dispersion or Channel Width (Å mm <sup>-1</sup> )	Useful Wavelength Range (Å)
SN 1969I					
1969 Dec. 13.....	568	Q1591	Schmidt	190	3400–6500
1970 Jan. 3.....	589	Q1640	Schmidt	190	3400–6500
1970 Jan. 5.....	591	MCSP	Oke	40/80*	3300–10600
1970 Jan. 14.....	600	MCSP	Oke	40/80	3300–10600
1970 Jan. 30.....	616	Q1713	Sargent	190	3900–6700
1970 Jan. 31.....	617	Q1745	Sargent	190	3900–6700
1970 Feb. 1.....	618	Q1773	Sargent	90	4100–6000
1970 Feb. 1.....	618	Q1774	Sargent	90	3700–4400
1970 Feb. 3.....	620	Q1811	Schmidt	190	3600–6700
1970 Aug. 8.....	806	Q2158	Gunn	190	3800–6700
1970 Aug. 8.....	806	Q2159	Gunn	190	3800–6700
1970 Sept. 7.....	836	Q2244	Schmidt	190	3800–6700
1970 Sept. 24.....	853	MCSP	Gunn	80/160	3600–10600
1971 Feb. 21.....	1003	MCSP	Gunn	80/160	4000–8000
SN 1970g					
1970 Aug. 4.....	802	MCSP	Oke	40/80	3300–10600
1970 Aug. 5.....	803	Q2133	Arp	190	3300–6700
1970 Aug. 5.....	803	Q2134	Arp	190	3800–6700
1970 Aug. 6.....	804	Q2140	Arp	190	3800–6700
1970 Aug. 6.....	804	Q2141	Arp	190	3800–6700
1970 Aug. 9.....	807	Q2161	Gunn	190	3800–6700
1970 Aug. 11.....	809	Q2178	Gunn	190	3800–6700
1970 Aug. 11.....	809	Q2179	Gunn	190	3800–6700
1970 Sept. 8.....	837	MCSP	Searle	40/80	3300–10600
1971 Apr. 15.....	1056	MCSP	Penston	80/160	3800–9000
1971 July 3.....	1135	MCSP	Penston	80/160	3800–8500

\* 40/80 denotes 40 Å channel widths for  $\lambda < 4950$  Å, 80 Å widths for  $\lambda > 5950$  Å.

## II. DATA

### a) *The Supernovae*

This paper estimates the distances to two recent Type II supernovae: 1969I in NGC 1058 and 1970g in M101 (NGC 5457). The supernova in the Sc galaxy NGC 1058 reached a maximum of  $B \simeq 13$  on about 1969 December 3 (Ciatti, Rosino, and Bertola 1971) and was very favorably located for observation, about 227" from the center of the galaxy. The observed recession velocity for NGC 1058 is  $+521$  km s<sup>-1</sup> (de Vaucouleurs 1967), which corresponds to a velocity of 665 km s<sup>-1</sup> as viewed from the center of our Galaxy.

The supernova in M101, also an Sc galaxy, was brighter, reaching  $B \simeq 11$  on about 1970 August 6 (Winzer 1974), but it was not so conveniently located, as it erupted in a large H II region, about 380" from the galaxy's center. The observed recession is  $+300$  km s<sup>-1</sup> (Humason, Mayall, and Sandage 1956), which corresponds to a galactocentric velocity of  $+415$  km s<sup>-1</sup>.

### b) *Spectra and Scans*

Table 1 lists the observational material gathered at the Hale Observatories: all the slit spectra were obtained with the Cassegrain image-tube spectrograph at the 200-inch (5-m) Hale reflector. As described in

KOPS, photometric scans were obtained at the Hale telescope with the multichannel spectrometer.

Figure 1 illustrates the evolution of the spectrum of SN 1969I with microphotometer density tracings, and shows 31 numbered features whose wavelengths are given in table 2. The wavelengths listed are for the minimum or maximum of the feature as measured either with a Grant measuring engine, or directly on the tracings. In either case, the uncertainty due to the width of the lines exceeds the measuring errors of a few angstroms. Table 2 also suggests identifications for some of the most prominent features. These are in accordance with those of KOPS, but differ from those of Ciatti *et al.* (1971). Those authors identify a large number of N II, He I, and He II lines, which we exclude principally on the grounds that they arise from atomic levels high above the ground state which would be populated only under conditions very different from those inferred by KOPS from the continuum temperatures. The trace for 1970 August 8 shows plainly the presence of [O I]  $\lambda 6300$ , which is the first clear evidence for this line in Type II supernovae. In KOPS, this line is present, but blended with H $\alpha$  due to the large bandwidth of the observations.

Figure 2 indicates that numbered features for SN 1970g, while table 3 gives the wavelengths. Since all the spectra were obtained at about the same time, the

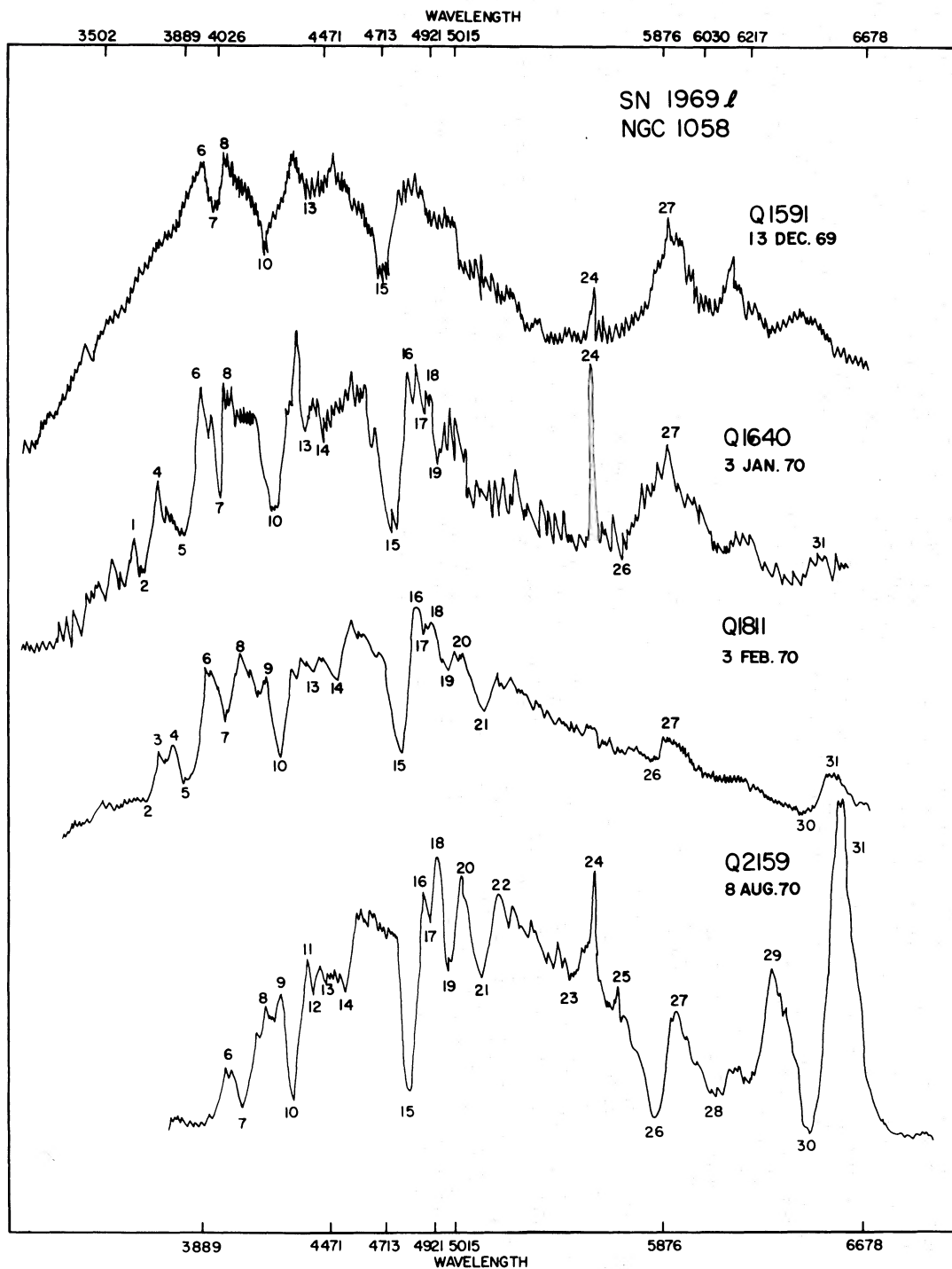


FIG. 1.—Microphotometer density tracings of SN 1969I in NGC 1058. The numbers near each tracing identify features whose wavelengths are listed in table 2. Features 10 and 15 ( $H\beta$  and  $H\gamma$ ) show the change from flat-bottomed to sharp absorption minima indicative of switching from optically thick to optically thin lines. Tracing Q2159 shows distinct [O I] emission at 6300 Å (feature 29).

TABLE 2  
MEASURED WAVELENGTHS: SN 1969I

Feature	Proposed Identification	Emission or Absorption	$\lambda_{rest}$	Q2244 (JD 836)	Q2159 (JD 806)	Q2158 (JD 806)	Q1811 (JD 620)	Q1774 (JD 618)	Q1773 (JD 617)	Q1745 (JD 617)	Q1713 (JD 616)	Q1640 (JD 589)	Q1591 (JD 568)
1	...	+	...	...	...	...	3679	...	...	...	...	3539	...
2	...	+	...	...	...	...	3753	3751	...	...	...	3690	...
3	...	+	...	...	...	...	3805	3810	...	...	...	3778	...
4	...	+	...	...	...	...	3875	3872	...	...	...	3853	...
5	Ca II	-	3950	...	...	...	...	...	...	...	...	...	...
6	Ca II	+	3950	3987	4003	3977	3977	3966	...	...	3981	3929	...
7	H $\delta$	+	4101	4063	4068	4032	4032	4046	...	...	4041	4022	3993
8	H $\delta$	-	4101	4170	4171	4092	4092	4097	...	...	...	4047	...
9	...	+	...	4253	4241	4235	4220	4217	4214	4219	4219	...	...
10	H $\gamma$	-	4340	4296	4290	4296	4269	4274	4259	4260	4270	4252	4211
11	H $\gamma$	+	4340	4355	4355	4358	4357	...	...	4350	...	...	...
12	...	-	...	4397	4387	4388	4357	...	4341	4367	...	...	...
13	...	-	...	...	4452	4440	4414	...	...	...	...	4390	4333
14	...	-	...	4541	4527	4531	4505	...	4501	4499	4504	4498	...
15	H $\beta$	-	4861	4805	4802	4801	4775	...	4777	4774	4776	4752	4712
16	H $\beta$	+	4861	4864	4864	4863	4841	...	...	4837	...	4846	...
17	...	-	...	4888	4886	4886	...	...	...	4876	...	4881	...
18	...	+	...	4930	4931	4928	...	...	...	4905	...	4902	...
19	...	-	...	4979	4982	4984	...	...	4963	4964	4965	4932	...
20	...	+	...	5028	5031	5033	...	...	...	5047	...	...	...
21	Mg I	+	5175	5116	5117	5117	5117	...	5109	5112	5111	...	...
22	Mg I	+	5175	5186	5181	5181	5117	...	...	5182	...	...	...
23	...	-	...	5485	5488	5488	...	...	...	...	...	...	...
24	Night sky	+	5577	5578	5576	5576	...	...	...	5575	...	5572	...
25	...	+	...	5702	5675	5679	...	...	...	...	...	...	...
26	Na I	+	5890	5822	5825	5836	5837	...	...	5817	5786	...	...
27	Na I	+	5890	5894	5916	5901	5881	...	...	...	...	5894	5913
28	...	-	...	6060	6061	6125	...	...	...	...	...	...	...
29	[O I]	+	6300	6300	6300	6300	...	...	...	...	...	...	...
30	H $\alpha$	-	6563	6445	6450	6442	6426	...	...	6430	6422	...	...
31	H $\alpha$	+	6563	6567	6564	6563	6546	...	...	6525	6523	6504	...

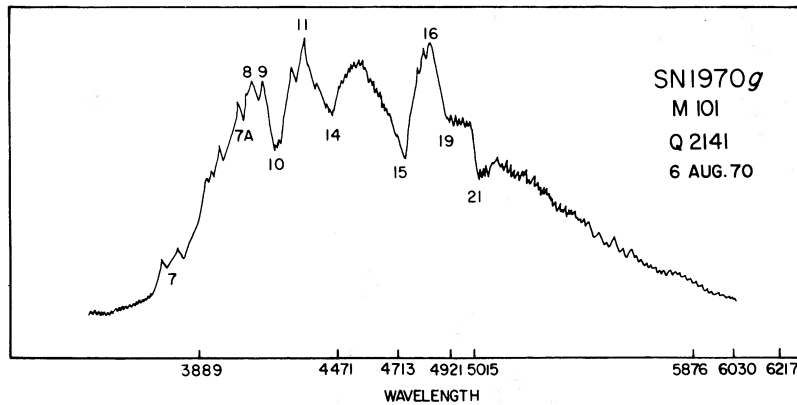


FIG. 2.—Microphotometer density tracings of SN 1970g in M101. The numbers refer to features whose wavelengths are listed in table 3.

individual spectra are not listed. Because that time was near maximum light, the continuum was especially strong, and few lines were visible, just as on 1969 December 13 for SN 1969l. The feature “7A” is seen in 1970g, but not in SN 1969l.

### c) Temperatures

The two scans in 1970 January of 1969l (KOPS) each exhibit a smooth continuum, which can be reasonably well approximated by a blackbody of  $T = 6000^\circ \pm 500^\circ$  K. In each scan, the continuum flux falls more rapidly than the blackbody shortward of about 4000 Å, which may be the combined effect of line blanketing and the Balmer jump. Thus, the temperatures refer principally to the region 10,000–5000 Å, where the fit is very good. When used with appropriate caution, the *UBV* photographic photometry of Ciatti *et al.* (1971) provides a measure of the temperature and luminosity at earlier times, where no scan is available.

The *B* and *V* colors for blackbodies derived by Matthews and Sandage (1963) can be described by the following equation:

$$10,000^\circ \text{K}/T = 1.59(B - V) + C, \quad (4)$$

where  $T$  is the temperature of the blackbody,  $B$  and  $V$  the usual blue and visual magnitudes, and  $C$  is a

TABLE 3  
MEASURED WAVELENGTHS: SN 1970g

Feature	Emission or Absorption	ID	$\lambda_{\text{rest}}$	$\lambda_{\text{meas}}$
7.....	—	Ca II	3950	3845
7A.....	—	...	...	4067
10.....	—	H $\gamma$	4340	4222
11.....	+			4339
14.....	—	...	...	4452
15.....	—	H $\beta$	4861	4740
18.....	+			4843
19.....	—	...	...	4914
21.....	—	Mg I	5175	5064
30.....	—	H $\alpha$	6563	6390
31.....	+			6503

constant which depends on the exact color system employed. For the Matthews and Sandage calibration,  $C = 0.70$ . Here, another calibration is established for the supernova in question. Using Ciatti *et al.*'s  $B - V = +0.75$  on January 7, and  $T = 6000^\circ$  K from the scans on January 5 and January 14,  $C$  is found to be 0.48 from equation (4). This new constant takes into account the color system used by Ciatti *et al.*, and the deviations from a blackbody introduced by lines in this particular supernova, especially in the *B*-band.

With this calibrated value of  $C$  and equation (4) the  $B - V$  magnitudes observed by Ciatti *et al.* are used to derive the photospheric temperature for each day of observation from 1969 December 3 to 1970 January 27. Using this derived blackbody temperature and the observed flux in the *V*-band, the angular size  $\theta$  is computed from equation (1). The results are shown in table 4 and in figure 3 where the expansion of the photosphere is manifest. For the purpose of determining  $D$ , the values of  $\theta = R/D$  are, with  $R$  in units of  $10^{15}$  cm and  $D$  in Mpc: JD 2,440,568,  $\theta = 0.039$  and JD 2,440,589,  $\theta = 0.115$ .

This method of determining  $\theta$  is far from ideal: it would be better to determine all the  $\theta$  from scans. Some change in  $B - V$  could be due to changes in line intensity rather than to changes in the continuum; the extrapolation of equation (4) from  $6000^\circ$  to  $20,000^\circ$  K in the early days of the supernova may not be justified. However, the evidence from spectra of this supernova is that the line intensities do not change radically at  $\lambda 4400$ , near the peak sensitivity of the *B*-band or at  $\lambda 5550$  near the peak of the *V*-band. Also, when equation (4) is actually utilized in the distance determination, the extrapolation extends only to about  $13,000^\circ$  K.

The supernova 1970g appeared in a large H II region of M101, which had previously been studied by Searle (1971), who determined its intrinsic reddening to be about  $A_v = 0.44$  mag. In the absence of any more specific information, this value is adopted, and the scans of August 4 and September 8 are compared with blackbodies which have been reddened by the Whitford relation (Miller and Mathews 1972). The temperatures are found to be  $9500^\circ \pm 500^\circ$  K for 1970 August 4, and  $5000^\circ \pm 500^\circ$  K for 1970 September 8. As for

TABLE 4  
BROAD-BAND MEASURES OF SN 1969I

Date	JD -2,440,000	$V$	$B - V$	$T$ ( $10^4$ ° K)	$R/D$ ( $10^{15}$ Mpc $^{-1}$ )
1969 Dec. 6.....	561	13.20	0.00	2.10	0.025
1969 Dec. 7.....	562	13.20	-0.05	2.50	0.021
1969 Dec. 8.....	563	13.25	+0.15	1.40	0.028
1969 Dec. 10.....	565	13.20	+0.20	1.26	0.038
1969 Dec. 11.....	566	13.30	+0.15	1.40	0.035
		13.20	+0.20	1.26	0.038
1969 Dec. 16.....	571	13.30	+0.20	1.26	0.039
1969 Dec. 26.....	581	13.35	+0.40	0.90	0.060
1969 Dec. 27.....	582	13.25	+0.55	0.74	0.087
1969 Dec. 29.....	594	13.45	+0.50	0.79	0.071
1970 Jan. 1.....	587	13.40	+0.65	0.66	0.102
1970 Jan. 2.....	588	13.35	+0.70	0.63	0.115
1970 Jan. 7.....	594	13.35	+0.75	0.60	0.129
1970 Jan. 25.....	612	13.40	+0.75	0.60	0.126
1970 Jan. 27.....	614	13.35	+0.75	0.60	0.129

1969I, the observed flux in the ultraviolet falls more rapidly than the blackbody curve, even when reddening is included. Photoelectric photometry by Winzer (1974) indicates  $B - V \simeq +0.29$  for about August 6, and  $B - V \simeq +0.87$  for September 1. If we assume  $T = 5700^\circ$  K for September 1 and  $E(B - V) \simeq 0.15$ , the equivalent of equation (4) can be obtained with these data. It is

$$10,000^\circ \text{ K}/T = 1.21(B - V) + 0.88, \quad (5)$$

where  $B - V$  has been corrected for extinction. The numerical coefficients are somewhat different from those for 1969I. This is due to the importance of changes in line intensities for 1970g. The August 4 observation shows a nearly featureless continuum near  $\lambda 4400$ , while the September 8 scan indicates a very strong absorption feature at  $\lambda 4400$ , which is of great importance in increasing the  $B$ -magnitude.

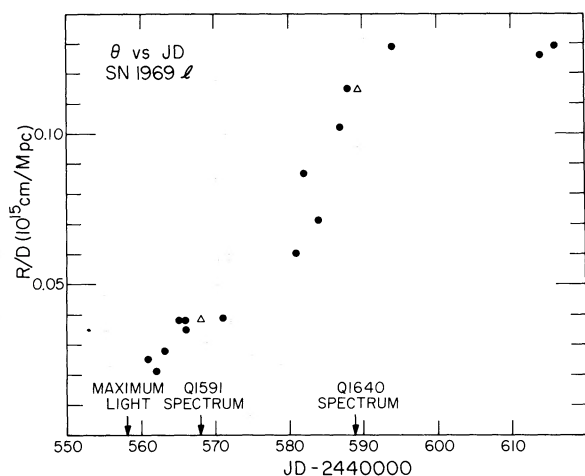


FIG. 3.—Angular size as a function of time. The angular sizes computed from broad-band observations are shown by filled circles (●), those adopted for the distance determination are shown as triangles (Δ).

Fortunately, the two scans of August 4 and September 8 are sufficiently separated in time so that they provide enough information for a distance estimate without the use of broadband data. The angular sizes at the two dates are  $\theta_1 = 0.144$  and  $\theta_2 = 0.285$  in units of  $10^{15}$  cm Mpc $^{-1}$ .

### III. LINE PROFILES AND PHOTOSPHERIC VELOCITY

This section shows how the velocity of the matter at the photosphere can be obtained from a study of the observed line profiles. The work of KOPS indicates that the radiation from a supernova consists of a broad continuum, with superposed P Cygni line profiles. Their results suggest that the supernova envelope consists of a photosphere with a scattering atmosphere above it. The shape of the P Cygni profiles indicates an expanding atmosphere: there is depletion of the continuum to the blue side of the line and contribution above the continuum to the red. It will be shown that the velocity of the matter at the photosphere corresponds to that velocity where the depletion of the continuum is the maximum, if the latter is sharp and well-defined, or if the latter exhibits a flat trough, to the velocity at the red edge of the depletion trough.

The following simple model of the photosphere and scattering atmosphere is considered: all the matter ejected from the supernova is assumed to be expanding radially and freely from a central point to explosion. Then the matter with velocity  $v$  travels a distance from the center  $R = vt$ , where  $t$  is the time since the explosion. The effective photosphere is located at the depth at which the continuum optical depth approaches unity. At that depth, the matter has a certain radial velocity  $v_{ph}$ . As the expansion progresses, the continuum radiation arises from layers deeper and deeper below the surface; simply put,  $v_{ph}$  decreases with  $t$ .

The radiation from the photosphere travels out through the expanding envelope until it is scattered. The scattering process can be viewed in two steps: first the primary absorption of the continuum photons, and second, the subsequent reemission of these photons.

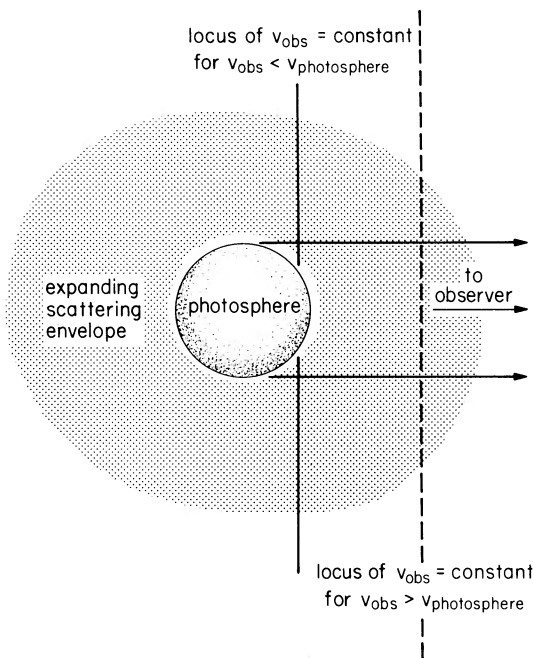


FIG. 4.—Schematic diagram of the expanding atmosphere in which resonant scattering takes place. The loci of constant observed velocities are shown in the case where  $v$  is proportional to  $r$ .

In the latter process the emitted photons may be absorbed again and reemitted several times if the line opacity is large. Consider first the primary absorption of the continuum radiation along the line of sight. There will be absorption by atoms moving toward the observer with velocities ranging from zero to the maximum expansion velocity. (In this discussion the relative motion between the center of expansion and the observer is ignored, though it is considered in analyzing the actual observations). Figure 4 shows a side view of the loci of atoms with velocities relative to the observer of  $v_{\text{obs}} < v_{\text{ph}}$  and  $v_{\text{obs}} > v_{\text{ph}}$ . In the simple case of  $v \propto R$  assumed at every instant in this model, the locus is a disk perpendicular to the line of sight. At each point of the envelope, the line opacity is the same along any path and is given by

$$\tau = (hc/4\pi)BN(R/v). \quad (6)$$

Here  $B$  is the Einstein absorption coefficient and  $N$  is the number of atoms per unit volume in the lower state of the resonance line at that point in space. The number density of atoms in the upper state of the transition is much smaller and can be neglected. Equation (6) depends on the assumptions that the thermal widths are much smaller than the widths due to mass motions (Castor 1970) and that  $N$  varies slowly over a velocity range of the order of the thermal velocity. In the present case, the radial velocities are typically  $\geq 3000 \text{ km s}^{-1}$ , while the thermal velocities of the scattering atoms are not more than  $\sim 10 \text{ km s}^{-1}$ ,

so that the two approximations above are clearly valid.

Although  $N$  changes slowly in one thermal velocity interval, it is a rapidly decreasing function of the expansion velocity. This can be demonstrated in two ways: first, the observed P Cygni profiles show that at the very blue edge of the profile, the depletion of the continuum decreases with increasing velocity. This result is possible only if  $N$  is a decreasing function of  $v$ . Second, even if the density is independent of velocity before free expansion begins, the subsequent motion would lead to a decreasing density distribution ( $N \propto v^{-2}$ ) at later times. In the model supernovae of Grassberg *et al.* (1971) the density is a decreasing function of velocity when free expansion begins, and their numerical calculations of supernova luminosities and expansion velocities are in qualitative accord with the observations of KOPS.

Consider the primary absorption of the continuum photons. It is clear from figure 4 that at observed velocities  $v_{\text{obs}} < v_{\text{ph}}$  the amount of absorption decreases with decreasing velocity because the area of the photosphere from which absorption is possible shrinks rapidly with decreasing velocity below  $v_{\text{ph}}$ . For  $v_{\text{obs}} > v_{\text{ph}}$  the amount of absorption at each velocity depends on the values of  $\tau$  on a surface of constant  $v_{\text{obs}}$ . With  $N$  a decreasing function of  $v$ , it is clear that, in the case when  $\tau \leq 1$  at each point in the envelope, the amount of absorption decreases with increasing velocity above  $v_{\text{ph}}$ . In this case, the primary absorption of continuum photons is greatest at  $v_{\text{ph}}$ . If  $\tau \geq 1$  at the inner part of the scattering envelope, the profile of the primary absorption exhibits a flat trough, with the velocity at the red edge of the absorption trough equal to  $v_{\text{ph}}$ . Figure 1 provides some evidence that this change actually takes place in the line profiles for H $\beta$  and H $\gamma$  (features 15 and 10). In the earliest spectrum Q1591, both lines have flat bottoms, while by Q1811, about 50 days later, the lines show the sharp cusps of optically thin lines.

The subsequent reemission of the absorbed photons does not alter these conclusions. In the case of  $\tau \leq 1$  everywhere, it can be derived analytically that for  $N$  decreasing faster than  $v^{-2}$ , the reemission of the absorbed photons does not shift the position of maximum depletion of the continuum as determined from the primary absorption alone. In this optically thin case, the emission profile of the reemission peaks at  $v = 0$ , and decreases symmetrically with larger and smaller observed velocities (when the slight asymmetry due to occultation of the far side of the envelope by the photosphere is ignored). The superposition of this emission profile and the primary absorption profile constitutes the observed P Cygni shape. If  $\tau \gg 1$  over large parts of the envelope, the emission is no longer symmetric about  $v_{\text{obs}} = 0$ . More emission is observed at  $v_{\text{obs}} < 0$  than at  $v_{\text{obs}} > 0$ , because at large optical depths, there is more backscattered radiation than forward-scattered radiation. For example, in the one-dimensional case in which radiation is only scattered forward or backward, the intensity of the backscattered beam is  $\tau/2$  times the forward-scattered intensity.

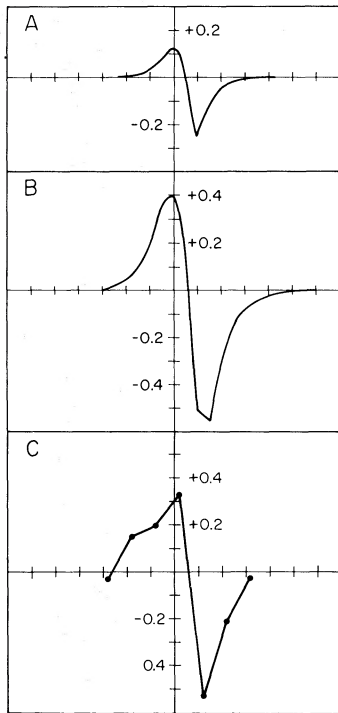


FIG. 5.—(a) Calculated line profile for an optically thin line. The graph shows  $(f_{\text{line}} - f_{\text{continuum}})/f_{\text{continuum}}$  versus velocity, where the unit is  $v_{\text{photospheric}}$ . Here  $v \propto r$ ,  $N \propto v^{-4}$ . (b) As in (a), but for an optically thick line  $\tau \leq 10$ . (c) H $\beta$  profile from scan of SN 1969l on 1970 Jan. 14. Here the velocity unit is  $4950 \text{ km s}^{-1}$ .

Caroff, Noerdlinger, and Scargle (1972) have considered the pertinent case of three-dimensional scattering in a rapidly expanding atmosphere. Their numerical results show that as the opacity is increased, there is indeed skewing of the scattered radiation to the red. However, as  $\tau$  is increased beyond about 3–5, they find that little additional asymmetry results. Thus in the case  $\tau \gg 1$  in the inner parts of the scattering envelope, the reemission of the primary absorbed photons may cause a rounding off of the depletion trough in the absorption profile. Nevertheless, in the resulting P Cygni profile, the matter velocity at the photosphere corresponds closely to the velocity observed at the red edge of the absorption trough.

The line profiles for various distributions of matter with velocity have been calculated, in a manner similar to that of Castor (1970). In figure 5, two of these

profiles are shown: in case A,  $\tau \leq 1$  throughout the envelope. In case B, the maximum value of  $\tau$  is 10, and  $N \propto v^{-4}$ , but no account is taken of the preferential backscattering, to demonstrate the maximum effect of optical depth on the absorption profile. The agreement between  $v_{\text{obs}}$  at the red edge of the observed absorption and  $v_{\text{ph}}$  is satisfactory. Also presented is an observed profile, case C. Each channel covers about  $4950 \text{ km s}^{-1}$  in velocity, which distorts the true profile somewhat. With appropriate adjustment of parameters theoretically calculated profiles can provide a good representation of the observed data.

It has been assumed in this section that the matter velocity at the photosphere  $v_{\text{ph}}$  is well defined. This is true when the photosphere has a sharp boundary where the continuum optical depth changes rapidly with respect to the velocity. Figure 3 demonstrates that the calculated angular size of the photosphere increased rapidly and smoothly during the first month of expansion. The assumption of a sharp photospheric boundary is most reliable during this interval, and the values of  $v_{\text{ph}}$  used in the distance determination are all obtained during that epoch.

#### d) Measured Values

Although the “red edge of the absorption minimum” is a somewhat vague prescription, in practice there is little ambiguity in measuring the appropriate quantity. The Balmer lines are used because they are prominent, unequivocally identified, and have relatively unimportant hyperfine splittings. The results given in table 5 are based on spectra for NGC 1058, and on a combination of spectra and scans for M101.

#### IV. DISTANCES

The distances to 1969l in NGC 1058 and 1970g in M101 can be obtained by employing the information in table 5 in equations (2) or (3). For NGC 1058, the use of  $v_{\text{ph}} = 8.6 \times 10^8 \text{ cm s}^{-1}$  and  $\theta = 0.039$  on JD 2,440,568 together with  $v_{\text{ph}} = 6.0 \times 10^8 \text{ cm s}^{-1}$  and  $\theta = 0.11$  on JD 2,440,589 in equation (3) gives a distance  $D = 12 \text{ Mpc}$  and  $t_0$  about JD 2,440,558. This  $t_0$  is close to the time of maximum light observed by Ciatti *et al.* (1971), although errors involved in its determination are too large to infer any cause for that coincidence. The photospheric radii implied by this distance are  $R = 0.47 \times 10^{15} \text{ cm}$  on JD 2,440,568 and  $R = 1.4 \times 10^{15} \text{ cm}$  on JD 2,440,589. The effect of an initial radius different from zero is to add  $0.34 \text{ Mpc}$  to the distance to NGC 1058 for every  $0.1 \times 10^{15} \text{ cm}$ .

TABLE 5  
PHOTOSPHERIC VELOCITIES

SN	Date*	$\theta$ †	Plate	H $\beta$ ‡	H $\gamma$ ‡	H $\delta$ ‡	Adopted‡	$V_{\text{galaxy}}$ ‡	$V_{\text{ph}}$ ‡
1969l.....	568	0.039	Q1591	8.5	7.8	...	8.1	0.5	$8.6 \pm 0.5$
1969l.....	589	0.115	Q1640	5.8	5.5	5.3	5.5	0.5	$6.0 \pm 0.5$
1970g.....	802	0.144	Q2141	7.1	7.1	...	7.1	0.3	$7.4 \pm 0.5$
1970g.....	837	0.285	Scan	3.8	4.5	...	4.0	0.3	$4.3 \pm 1.0$

\* Julian date  $-2,440,000$ . †  $\theta$  in units of  $10^{15} \text{ cm Mpc}^{-1}$ . ‡ All velocities in units of  $10^8 \text{ cm s}^{-1}$ .

Since no presupernova star was visible at the site of the eruption, the initial radius is likely to be smaller than  $0.1 \times 10^{15}$  cm, and the error introduced in the distance determination is negligible.

For M101, using the data from table 5 for  $v_{ph}$  and  $\theta$ , the distance to M101 is about 6.5 Mpc. The photospheric radius on JD 2,440,837 is  $1.8 \times 10^{15}$  cm, and the initial time is about JD 2,440,788. This is 16 days before maximum, which indicates the uncertainty in the relation between  $t_0$  and the time of maximum light.

## V. DISCUSSION

### a) Distances and Magnitudes

The distances derived here agree surprisingly well with the extragalactic distance scale of Sandage and Tammann (1973), who propose distances of 7.2 Mpc to the group containing M101, and 13.9 Mpc to the group containing NGC 1058. To determine whether this agreement is mere coincidence or true convergence requires an estimate of the errors inherent in the supernova distances.

The temperatures derived from scans are probably good to 500° K, but those from broad-band colors may have substantially larger errors. The resulting values of  $\theta$  may vary by 20 percent. The velocities are well determined in the cases where a spectrum was employed, but have significant errors where a scan was used. If the theory of § III is reliable, the distances are only subject to about 10 percent uncertainty from this source when spectra are used, and about 30 percent when a scan is used. The effects of a nonzero  $R_0$  are less than 5 percent, for  $R_0 < 10^{14}$  cm.

Considering the data actually employed, the errors incurred in the M101 distance imply  $D = 6 \pm 3$  Mpc and those for NGC 1058 imply  $D = 12 \pm 3$  Mpc, so the agreement with Sandage and Tammann (1973) is no accident. The recession velocities of the two individual galaxies correspond to a Hubble constant of  $H = 60 \pm 15$ , while the mean recession velocities for the groups in which they are located (Sandage and Tammann 1973; Materne 1974) give very nearly the same Hubble constant.

The temperature and radius data for 1970g give clear evidence of decreasing luminosity: for JD 2,440,802,  $L = 4\pi R^2 \sigma T^4 = 4.64 \times 10^{42}$  ergs  $s^{-1}$ , while for JD 2,440,837  $L = 1.44 \times 10^{42}$  ergs  $s^{-1}$ . Even though the spectrum is not really blackbody, most of the energy emitted at these epochs is observed in the band 10,000–3300 Å. This result contradicts the prediction based on a simple pulsar-powered supernova, where the luminosity remains nearly constant (Ostriker and Gunn 1971).

The observed magnitude and the distance can be used to estimate the absolute magnitude near maximum light. For NGC 1058, if  $m_B = 13.0$  and  $D = 12$  Mpc,

then  $M_B = -17.4$  and for M101, if  $m_B \simeq 11.0$  and  $D = 6$  Mpc,  $M_B = -17.9$ . Thus, despite some crudeness of the estimate, the absolute magnitudes of these two Type II supernovae were quite similar.

The method described in this paper is superficially similar to that of Branch and Patchett (1973) for Type I supernovae. The method here has some advantages in that it refers to observations made of a single object, rather than a collection of observations and extrapolations for all supernovae of a given kind. Also, somewhat arbitrary factors such as the “center-to-limb effects” and the ratio of “photospheric velocity” to “actual velocity of ejected material” are replaced by a model of line formation. Last, the identifications of the Type II lines used here are not disputed so that the rest wavelengths are known, while the Si II line identified in Type I by Branch and Patchett is less certain.

### b) Improvements

Most of the errors inherent in this method of distance determination could be removed by carefully planned observations. If the temperature and flux density were measured several times, and spectra taken on consecutive nights, the distance would be highly overdetermined, observational errors would become unimportant, and only the systematic errors would remain. This could be done with a well-equipped 2-m telescope to magnitude 15 using conventional technology, and to a considerably fainter limit with an efficient photon counting spectrograph.

With an ordinary photoelectric scanner, or photometer with appropriate filters, the flux could be measured in two bands which are free of lines. For example, the bands  $\lambda\lambda 7000-7500$  and  $\lambda\lambda 5250-5500$  would be suitable for Type II supernovae. This color defines a temperature, and the flux would permit an estimate of  $\theta$ . If spectra are available on neighboring nights,  $v_{ph}$  can be found from the red edge of absorption minima. It is important that the observations be obtained during the first month after maximum; the expansion of the photosphere is not simple at later times, as illustrated by the flattening of figure 3.

It is not unreasonable to expect that the application of this method to supernovae in the local supercluster could provide an independent and accurate estimate of the Hubble constant, and the absolute magnitude of supernovae.

Our deepest thanks to the many observers who so generously shared their data that this investigation might be carried out, and especially to L. Searle and J. B. Oke for their assistance and advice. R. P. K. is grateful for an NSF Fellowship and a Virginia Steele Scott Fellowship. J. K. is supported by the National Science Foundation grant GP-16147A.

## REFERENCES

- Baade, W. 1926, *Astr. Nachr.*, **228**, 359.  
 Branch, D., and Patchett, B. 1973, *M.N.R.A.S.*, **161**, 71.  
 Caroff, L. J., Noerdlinger, P. D., and Scargle, J. D. 1972, *Ap. J.*, **176**, 439.  
 Castor, J. I. 1970, *M.N.R.A.S.*, **149**, 111.  
 Ciatti, F., Rosino, L., and Bertola, F. 1971, *Mem. Soc. Astr. Italia*, **42**, 163.  
 de Vaucouleurs, G. 1967, *A.J.*, **72**, 730.

- Grassberg, E. K., Imshennik, V. S., and Nadyozhin, D. K. 1971, *Ap. and Space Sci.*, **10**, 28.  
Humason, M. L., Mayall, N. U., and Sandage, A. R. 1956, *A.J.*, **61**, 97.  
Kirshner, R. P., Oke, J. B., Penston, M., and Searle, L. 1973, *Ap. J.*, **185**, 303.  
Materne, J. 1974, preprint.  
Mathews, T. A., and Sandage, A. R. 1963, *Ap. J.*, **138**, 30.  
Miller, J. S., and Mathews, W. G. 1972, *Ap. J.*, **172**, 593.  
Ostriker, J. P., and Gunn, J. E. 1971, *Ap. J. (Letters)*, **164**, L95.  
Sakurai, A. 1960, *Comm. in Pure and Appl. Math.*, **13**, 353.  
Sandage, A. R. 1956, *Ap. J.*, **125**, 436.  
Sandage, A. R., and Tammann, G. 1973, private communication.  
Searle, L. 1971, *Ap. J.*, **168**, 327.  
Winzer, J. E. 1974, *J.R.A.S. Canada*, **68**, 36.

ROBERT P. KIRSHNER: California Institute of Technology, 1201 California Boulevard, Pasadena, CA 91109

JOHN KWAN: Institute for Advanced Study, Princeton, NJ 08540